

RADAR: Robust Two-stage Modality-incomplete Industrial Anomaly Detection

Bingchen Miao, Wenqiao Zhang, Juncheng Li, Siliang Tang, Zhaocheng Li, Haochen Shi, Jun Xiao, Yueting Zhuang

Zhejiang University

Abstract

Multimodal Industrial Anomaly Detection (MIAD), utilizing 3D point clouds and 2D RGB images to identify the abnormal region of products, plays a crucial role in industrial quality inspection. However, the conventional MIAD setting presupposes that all 2D and 3D modalities are paired, overlooking the fact that multimodal data collected from the real world is often imperfect due to modality-missing. Consequently, MIAD models that demonstrate robustness against modality-incomplete data are highly desirable in practice. To address this challenge, we introduce a first-of-its-kind study that comprehensively investigates Modality-Incomplete Industrial Anomaly Detection (MIAD), to consider the imperfect learning environment in which the multimodal information is incomplete. Not surprisingly, we discovered that most existing MIAD approaches are inadequate, leading to significant performance degradation on the MIAD benchmark we developed. In this paper, we propose a novel two-stage **Robust modAlity-aware fusing and Detecting frAmewoRk**, abbreviated as **RADAR**. Our bootstrapping philosophy is to enhance two stages in MIAD, improving the robustness of the Multimodal Transformer: i) In feature fusion, we first explore learning modality-incomplete instruction, guiding the pre-trained Multimodal Transformer to robustly adapt to various modality-incomplete scenarios, and implement adaptive parameter learning based on a HyperNetwork; ii) In anomaly detection, we construct a real-pseudo hybrid module to highlight the distinctiveness of modality combinations, further enhancing the robustness of the MIAD model. Our experimental results demonstrate that the proposed RADAR significantly surpasses conventional MIAD methods in terms of effectiveness and robustness on our newly created MIAD dataset, underscoring its practical application value.¹

Introduction

Industrial Anomaly Detection (IAD) is pivotal in industrial quality inspection, primarily focusing on identifying product defects. A significant challenge in this domain is the *intrinsic population bias*² between normal and abnormal examples. Consequently, most current IAD approaches adopt an unsupervised learning framework, *i.e.*, training models solely on anomaly-free examples and testing them on

¹Our project is available at <https://anonymous.4open.science/r/RADAR-54F2>.

²In industrial settings, normal products vastly outnumber defective ones, making anomalies relatively rare.

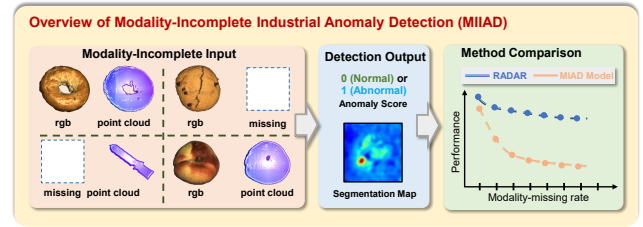


Figure 1: Outline of MIIAD. MIIAD involves input data with incomplete modalities, generating anomaly scores and segmentation maps as detection results. Most existing MIAD methods struggle to tackle the challenges of MIIAD. In contrast, our model RADAR significantly outperforms these methods, demonstrating robust MIIAD capability.

both normal and defective examples during inference. Moreover, most previous IAD methods relied heavily on 2D imagery (Gudovskiy, Ishizaka, and Kozuka 2022; Roth et al. 2022b; Defard et al. 2021a). However, recent studies (Wang et al. 2023b) highlight the importance of both 3D geometries and the color characteristics from 2D images in identifying defects, suggesting that developing systems that integrate 3D point clouds with 2D images represent a promising pathway toward achieving high-performance in IAD.

The advent of multimodal transformers has revolutionized multimodal learning across various fields, offering promising solutions for multimodal industrial anomaly detection. Nonetheless, these approaches often presume complete data availability (Ma et al. 2022a), an assumption rarely feasible in industrial contexts due to equipment limitations and privacy concerns, particularly with 3D data acquisition. The lack of data modalities, whether during training or testing, can detrimentally affect system performance. These observations underscore the urgent need for robust detection methods that effectively handle multimodal data and adapt to various conditions of modality incompleteness. Currently, there is a notable gap in advancing methods that can robustly operate under such modality-incomplete settings.

To bridge the gap, we introduce a novel and demanding task: **Modality-Incomplete Industrial Anomaly Detection (MIAD)**. Alongside this, we propose a comprehensive benchmark designed to simulate scenarios in which

various missing-modality cases may occur in any data samples, such as accessing only 2D RGB images or 3D point clouds, during either the training or testing phases. To facilitate robust detection in such an imperfect environment, we propose a novel **Robust modALity-missing fusing and Detecting frAmewoRk**, dubbed **RADAR**. RADAR enhances the model’s ability to handle incomplete modalities at the feature fusion stage, incorporating three main components: **Pre: 2D&3D Feature Extraction:** We utilize the MaskTransformer for extracting 3D point cloud features, and the Vision Transformer (ViT) for 2D RGB image features. **Stage1: Adaptive Instruction Fusion:** We construct modality-incomplete instruction to highlight multimodal transformers with missing modalities, allowing them to adapt robustly to various scenarios of modality-incomplete. We also employ HyperNetwork to derive an adaptive modality-aware fusion mechanism, whose parameters are dynamically generated depending on the 2D and 3D modality representation. **Stage2: Real-Pseudo Hybrid Detection:** We design a Real-Pseudo Hybrid Module to highlight the distinctiveness of modality combinations, further enhancing the robustness of the framework. Finally, we integrate the features stored in the three repositories and make decisions based on the Mahalanobis distance matrix (MDM) and One-Class Support Vector Machine (OCSVM).

Our contributions are three-fold:

- We present a new challenging and practical task: Modality-incomplete Industrial Anomaly Detection (MIAD), together with one newly designed benchmark.
- We propose an end-to-end MIAD learning framework, called RADAR, enhancing the robustness of the multimodal transformer in the absence of modalities.
- Through extensive experiments, we show that our method improves all the prevalent multimodal industrial anomaly detection line-ups on MIAD benchmarks.

Related Work

Industrial Anomaly Detection

2D Industrial Anomaly Detection can be categorized as follows. **i) Feature Extraction Method:** It’s typical approaches including the utilization of teacher-student architecture and one-class classification methods. The teacher-student architecture (Bergmann et al. 2020; Salehi et al. 2021; Wang et al. 2021a) leverages pre-trained models to impart knowledge from a teacher network to a student network, comparing their outputs during the inference stage to determine the anomalous data. One-class classification (OCC) (Zhang and Deng 2021; Hu, Chen, and Shao 2021) determines abnormality based on relative feature positions of the test sample’s features and the hypersphere, sometimes augmented by artificially created abnormal samples. **ii) Reconstruction-based Method:** It utilizes self-trained encoders and decoders to reconstruct images for anomaly detection, demonstrating strong performance in pixel-level anomaly identification. Existing reconstruction models include autoencoders (Bergmann et al. 2018; Dehaene and Eline 2020; Wang et al. 2020), GANs (Song et al. 2021;

Liang et al. 2023), transformer (Mishra et al. 2021; Jiang et al. 2022) and diffusion models (Wyatt et al. 2022).

3D Industrial Anomaly Detection offers advantages in capturing spatial information beyond what is available in RGB images. The release of the MVTEC 3D-AD dataset (Bergmann et al. 2022a) has spurred several papers focusing on anomaly detection in 3D industrial images. Bergmann and Sattlegger (Bergmann and Sattlegger 2023a) introduced a teacher-student model for 3D anomaly detection, while Horwitz and Hoshen (Horwitz and Hoshen 2023) proposed a method that combines hand-crafted 3D representations with 2D features.

Modality-incomplete Learning

Traditional models often struggle when input data lacks one or more modalities, which is common in real-world scenarios due to constraints in data collection, privacy concerns, or technical limitations. Techniques such as variational autoencoders (Chartsias et al. 2017; van Tulder and de Bruijne 2018) have been particularly popular for their ability to generate missing modalities in an unsupervised manner.

However, these approaches often neglect the nuanced distinctions between shared features and modality-specific features, which are crucial for optimizing model performance in multi-modal settings (Wang et al. 2023a). Robust-Mseg (Chen et al. 2019) addresses missing modalities by disentangling features into modality-specific appearance codes and modality-invariant content codes. SMIL (Ma et al. 2021a) leverages Bayesian meta-learning to achieve flexibility and efficiency in handling incomplete training and testing data. ShaSpec (Wang et al. 2023a) introduces a simpler yet potent architecture, focusing on the classification, segmentation, distribution alignment, and domain classification tasks. We followed the settings for modality-missing in these recognized works to ensure the generality of our method.

In contrast, these methods typically utilize a single feature fusion stage, whereas our approach incorporates two stages to enhance the framework’s robustness.

Methodology

This section introduces the **Robust modALity-imcomplete fusing and Detecting frAmewoRk (RADAR)** for MIAD. We will begin by outlining the task and the RADAR model. Following that, we will provide a detailed explanation of each module within the framework.

Overview

Task Formulation. We consider MIAD which involves two modalities: 2D RGB image and 3D point cloud. Specifically, a MIAD dataset, denoted as \mathcal{D} , can be divided into three subsets based on the modality missing situations: $\mathcal{D} = \{\mathcal{D}^C, \mathcal{D}^{2D}, \mathcal{D}^{3D}\}$. Here, $\mathcal{D}^C = \{(x_i^{2D}, x_i^{3D}, y_i)\}$ ($i \in 1, \dots, |\mathcal{D}^C|$) represents the modality-complete subset, $\mathcal{D}^{2D} = \{(x_i^{2D}, y_i)\}$ ($i \in 1, \dots, |\mathcal{D}^{2D}|$) comprises samples missing 3D point clouds, and $\mathcal{D}^{3D} = \{(x_i^{3D}, y_i)\}$ ($i \in 1, \dots, |\mathcal{D}^{3D}|$) includes samples lacking 2D RGB images. The task objective is to effectively perform IAD in various modality-incomplete settings.

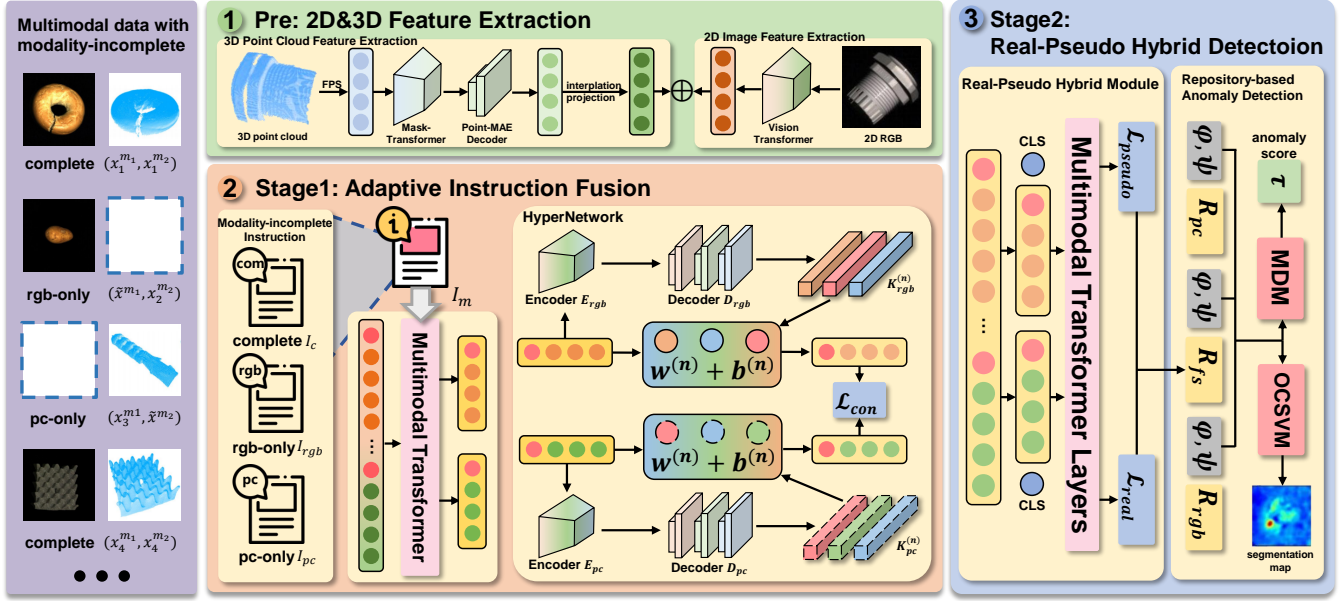


Figure 2: **Overview of RADAR.** It consists of three parts: **i) 2D&3D Feature Extraction.** Leveraging ViT and MaskTransformer to extract features of 2D RGB images and 3D point clouds, respectively. **ii) Adaptive Instruction Fusion.** Prepending the modality-incomplete instruction I_m of multimodal data $(x_i^{m_1}, x_i^{m_2})$ into a simple Multimodal Transformer input token, while introducing HyperNetwork to achieve adaptive parameter learning. **iii) Real-Pseudo Hybrid Detection.** Constructing a Real-Pseudo Hybrid Module for further fusion and feeding the features stored in multiple repositories R_{rgb} , R_{fs} , and R_{pc} into the MDM and OCSVM for hybrid decisions on anomaly score τ and segmentation map, respectively.

Framework Overview. As illustrated in Fig. 2, the RADAR framework addresses the practical MIIAD challenge through three main components: **Pre: 2D&3D Feature Extraction.** We extract features from 2D RGB images and 3D point clouds utilizing the ViT and the MaskTransformer. **Stage1: Adaptive Instruction Fusion.** We employ the modality-incomplete instruction and HyperNetwork to facilitate adaptive learning of robust feature fusion. **Stage2: Real-Pseudo Hybrid Detection.** We design a Real-Pseudo Hybrid Module to highlight the distinctiveness of modality combinations for further robust fusion and connect features from three repositories to make decisions based on MDM and OCSVM.

Pre: 2D&3D Feature Extraction

2D Image Feature Extraction. We employ pretrained ViT (Dosovitskiy et al. 2021) from HuggingFace (Wolf et al. 2020) to extract 2D image features f_{rgb} , consistent with previous research. Due to space constraints, further details will not be provided.

3D Point Cloud Feature Extraction. The input point cloud \mathcal{P} is an unordered sequence of point positions in three-dimensional space, containing $N_{\mathcal{P}}$ points, which makes it challenging to extract meaningful features directly by feeding them into standard Transformer modules. We first divide the point cloud \mathcal{P} into M groups $\mathcal{P} = \{\mathcal{P}_1, \dots, \mathcal{P}_M\}$ using Farthest Point Sampling (FPS) (Qi et al. 2017). For each group \mathcal{P}_i , we further extract feature vector \mathcal{T}_i utilizing a pretrained MaskTransformer (Yu et al. 2022) and Point-MAE (Pang et al. 2022), *i.e.*, each group \mathcal{P}_i has a single

point feature \mathcal{T}_i . We take the output of the MaskTransformer as the initial point features $\mathcal{T}_{en} = [\mathcal{T}_{en1}, \dots, \mathcal{T}_{enM}]$. \mathcal{T}_{en} will be fed to Point-MAE to further improve the 3D point feature and take the decoder’s output as the extracted 3D point features $\mathcal{T} = [\mathcal{T}_1, \dots, \mathcal{T}_M]$, which can be denoted as $\mathcal{T} = Decoder_{MAE}(\mathcal{T}_{en})$.

Point Interpolation and Projection. To prevent the imbalanced feature density issue caused by FPS, we interpolate the features back into the original point cloud, which can be denoted as

$$p'_j = \sum_{i=1}^M \alpha_i \mathcal{T}_i, \quad \alpha_i = \frac{\frac{1}{\|c_i - p_j\|_2 + \epsilon}}{\sum_{k=1}^M \sum_{t=1}^{N_{\mathcal{P}}} \frac{1}{\|c_k - p_t\|_2 + \epsilon}}, \quad (1)$$

where $p_j, j \in \{1, 2, \dots, N_{\mathcal{P}}\}$ represents a point in the original point cloud data, $p'_j, j \in \{1, 2, \dots, N_{\mathcal{P}}\}$ denotes the point after interpolation, c_i is the center point associated with the corresponding group \mathcal{P}_i , and ϵ is a fairly small constant. Subsequently, we apply average pooling and additional operations to derive 3D point cloud features f_{pc} .

Stage1: Adaptive Instruction Fusion

Modality-incomplete can result in a performance decrease in Multimodal Transformers or feature extraction models (Lee et al. 2023). In the first stage, inspired by prompt learning, we propose introducing modality-incomplete instruction into the Multimodal Transformer for feature fusion to preliminarily enhance robustness in MIIAD.

Modality-incomplete Instruction. We initially create specific modality-incomplete instructions for each modality-

incomplete scenario. For IAD tasks involving two modalities, we configure $2^2 - 1 = 3$ instructions and prepend them into the input tokens based on the modality-incomplete condition. The input embedding feature of the j -th MSA layer is denoted as $h^j \in \mathbb{R}^{L_i \times d}$, $i = 1, 2, \dots, N$ with an input length L_i and dimension of d . Importantly, the insertion of instructions can also be extended in multiple layers, denoted as $I_m = \{i_m^j\}_{j=start}^{end} \in \mathbb{R}^{N_i \times L_i \times d}$, where i_m^j represents the input sequence linked to the j -th layer in the Transformer. Function $f_{instruct}$ describing the process of adding these instructions can be denoted as

$$f_{instruct}(i_m^j, h^j) = \text{concat}(i_m^j; h^j), \quad (2)$$

It enables the current layer to connect with that of the previous layer. Such interaction can effectively enhance the model’s robustness in addressing modality-incomplete.

Instruction Feature Fusion. Modality feature fusion is pivotal in multimodal tasks, and a model’s performance in such tasks heavily relies on the fusion degree of modality features (Zhao et al. 2023; Gong et al. 2023; Lee et al. 2023). We devised a concise Multimodal Transformer incorporating modality-incomplete instruction to adeptly guide the model in addressing IAD robustly.

Our Multimodal Transformer straightforwardly combines the concatenation results T_{fs} of f_{pc} and f_{rgb} as input. Subsequently, it appends the modality-incomplete instruction $i_m^j \in \mathbb{R}^{L_i \times d}$ to the j -th layer. These instructions are then prepended to the feature embedding to produce the modified feature Tex_i^j , which can be represented as

$$Tex_i^j = f_{instruct}(i_m^j, h^j), \quad (3)$$

The feature Tex_i^j has robustness against incomplete modalities, indicating the completion of preliminary feature fusion. Afterwards, this feature will divide into two new modality features $\{\hat{f}_{pc}, \hat{f}_{rgb}\}$ based on the instruction length.

The features of the two modalities are mapped to feature $\{g_{pc}, g_{rgb}\}$ via Multi-Layer Perceptrons (MLP) MLP_{pc} and MLP_{rgb} , along with fully connected layers. The ultimate feature fusion learning is conducted using patch-wise contrastive loss, specifically the InfoNCE Loss (van den Oord, Li, and Vinyals 2018), serving as the objective function, which can be formulated as

$$L_{con} = \frac{g_{pc} \cdot g_{rgb}^T}{\sum_{t=1}^{N_b} \sum_{k=1}^{N_p} g_{pc} \cdot g_{rgb}^T}, \quad (4)$$

where N_b is the batch size, and N_p is the patch number.

HyperNetwork-based Adaptive Learning. We suggest utilizing the HyperNetwork (Ha, Dai, and Le 2017) to enable adaptive parameter learning for MLP_{pc} and MLP_{rgb} . More precisely, the HyperNetwork treats the MLP parameters as a matrix $K^{(n)} \in \mathbb{R}^{N_{in} \times N_{out}}$, where N_{in} and N_{out} denote the number of input and output neurons in the n -th layer of the MLP, respectively. The creation process of $K^{(n)}$ can be viewed as matrix factorization, illustrated as

$$K^{(n)} = \xi(z^{(n)}; \Theta_p), \quad (5)$$

where $z^{(n)}$ and $\xi(\cdot)$ are randomly initialized with parameter Θ_p during the training process. The backpropagation of

gradients is used to update $z^{(n)}$ and $\xi(\cdot)$. Subsequently, a layer-specific encoder $\xi^h(\cdot)$ encodes $\{\hat{f}_{pc}, \hat{f}_{rgb}\}$ as e^h . And we employ HyperNetwork to transform the embedded $e^{(n)}$ into parameters; in other words, we feed $e^{(n)}$ into the following two MLP layers to generate adaptive parameters

$$w^{(n)} = (W_1 \xi^h(e^h) + B_1)W_2 + B_2, \quad (6)$$

where W_1 , W_2 , B_1 , and B_2 , are the weights and bias terms of the first and second MLP layers, respectively. Then the model will adaptively adjust parameters based on diverse inputs, thereby substantially bolstering robustness.

Stage2: Real-Pseudo Hybrid Detection

In the second stage, we believe that if a sample is frequently misclassified, it may indicate the presence of ambiguous information (Zhang, Doughty, and Snoek 2023). To further strengthen the robustness of the framework, we propose a Real-Pseudo Hybrid Module to highlight the distinctiveness of different modality combinations. Finally, based on the three repositories for storing features, we utilize MDM and OCSVM for anomaly detection decision.

Real-Pseudo Hybrid Module. We divide the multimodal feature representation \hat{G} into two groups, denoted as \hat{G}_{real} and \hat{G}_{pseudo} , and input them into a Multimodal Transformer layer. This allows the two groups of features to be trained under different supervision, enabling the learning of diverse semantic information. Considering practical utility, we eliminate the attention operation, thus the output attention is

$$a_{ij} = \frac{I_{ij} \exp(\frac{q_i^T k_j}{\sqrt{D}})}{\sum_{\{j', I_{ij'}=1\}} \exp(\frac{q_i^T k_{j'}}{\sqrt{D}})}, \quad (7)$$

where q and k represent the query and key, while i and j denote the i -th and j -th tokens in the query and key. D represents the dimensionality of the key.

For data trained with real labels, we simply use the standard cross-entropy loss for classification and L2 loss for regression, denoted as L_{real} . For data trained with pseudo-labels, we average the unimodal predictions across training epochs to obtain modality-specific pseudo-labels. We then use KL divergence loss for classification tasks and L2 loss for regression tasks, denoted as L_{pseudo} .

Repository-based Anomaly Detection. Subsequently, we opt to employ multiple repositories to house features, aligning with prevalent practices in advanced IAD methodologies in recent years. The 3D point cloud features, 2D RGB image features, and modality fusion features will be stored in repository R_{pc} , R_{rgb} , and R_{fs} respectively. These repositories facilitate hybrid anomaly detection decisions, with each repository capable of generating predicted anomaly scores and segmentation maps. The initial hybrid results exported from the repositories can be depicted as

$$S\hat{c}o_a = \{\phi(R_{pc}, f_{pc}), \phi(R_{rgb}, f_{rgb}), \phi(R_{fs}, f_{fs})\}, \quad (8)$$

$$S\hat{e}g_m = \{\psi(R_{pc}, f_{pc}), \psi(R_{rgb}, f_{rgb}), \psi(R_{fs}, f_{fs})\}, \quad (9)$$

Table 1: P-AUROC score for anomaly detection of MIIAD Dataset with 3D point cloud modality missing. A larger score indicates better performance. We color each row as the **best**, **second best**, and **third best**.

Missing rate	Methods	MIIAD Dataset										
		Bagel	Cable Gland	Carrot	Cookie	Dowel	Foam	Peach	Potato	Rope	Tire	Mean
30%	Voxel GAN (Bergmann et al. 2022b)	0.542	0.576	0.534	0.577	0.522	0.565	0.498	0.569	0.594	0.516	0.547
	Voxel VM (Bergmann et al. 2022b)	0.431	0.454	0.417	0.436	0.405	0.443	0.387	0.468	0.479	0.408	0.426
	PatchCore+FPFH (Horwitz and Hoshen 2022)	0.758	0.779	0.797	0.776	0.755	0.752	0.729	0.776	0.832	0.765	0.771
	AST (Rudolph et al. 2023)	0.742	0.766	0.788	0.773	0.729	0.731	0.714	0.753	0.819	0.747	0.758
	M3DM (Wang et al. 2023b)	0.754	0.782	0.795	0.783	0.747	0.755	0.731	0.777	0.835	0.763	0.772
	RADAR (Ours)	0.794	0.803	0.832	0.805	0.784	0.769	0.758	0.811	0.872	0.797	0.813
50%	Voxel GAN (Bergmann et al. 2022b)	0.456	0.432	0.467	0.516	0.489	0.466	0.417	0.515	0.524	0.429	0.458
	Voxel VM (Bergmann et al. 2022b)	0.372	0.366	0.375	0.413	0.377	0.334	0.346	0.428	0.437	0.344	0.376
	PatchCore+FPFH (Horwitz and Hoshen 2022)	0.664	0.647	0.738	0.747	0.675	0.714	0.622	0.726	0.768	0.667	0.696
	AST (Rudolph et al. 2023)	0.643	0.631	0.729	0.724	0.667	0.696	0.604	0.713	0.742	0.648	0.668
	M3DM (Wang et al. 2023b)	0.659	0.650	0.739	0.745	0.681	0.714	0.617	0.728	0.767	0.671	0.693
	RADAR (Ours)	0.713	0.673	0.752	0.773	0.752	0.719	0.682	0.750	0.794	0.723	0.735
70%	Voxel GAN (Bergmann et al. 2022b)	0.397	0.385	0.422	0.465	0.443	0.427	0.356	0.478	0.469	0.387	0.395
	Voxel VM (Bergmann et al. 2022b)	0.323	0.307	0.346	0.379	0.324	0.298	0.307	0.386	0.393	0.306	0.332
	PatchCore+FPFH (Horwitz and Hoshen 2022)	0.610	0.617	0.691	0.627	0.635	0.652	0.593	0.622	0.696	0.585	0.636
	AST (Rudolph et al. 2023)	0.595	0.601	0.677	0.614	0.615	0.635	0.581	0.607	0.683	0.566	0.613
	M3DM (Wang et al. 2023b)	0.613	0.620	0.689	0.634	0.636	0.647	0.594	0.629	0.702	0.578	0.639
	RADAR (Ours)	0.653	0.624	0.723	0.670	0.661	0.705	0.630	0.645	0.741	0.617	0.684

Table 2: Ablation study of different modules. F, A, and R represent 2D&3D Feature Extraction, Adaptive Instruction Fusion, and Real-Pseudo Hybrid Detection, respectively.

Method	Setting			MIIAD Dataset		
	FE	AIF	RPHD	P-AUROC	AUPRO	I-AUROC
Baseline				0.639	0.303	0.842
+ FE	✓			0.648	0.316	0.851
+ AIF		✓		0.662	0.329	0.856
+ RPHD			✓	0.658	0.335	0.857
+ FE & AIF	✓	✓		0.669	0.344	0.863
+ FE & RPHD	✓		✓	0.671	0.339	0.864
+ AIF & RPHD		✓	✓	0.677	0.353	0.873
RADAR (Ours)	✓	✓	✓	0.684	0.368	0.877

where ϕ, ψ is the score function introduced in PatchCore (Roth et al. 2022b), which can be formulated as

$$\phi(R, f) = \eta \|\hat{f}^* - r^*\|_2, \quad (10)$$

$$\psi(R, f) = \{\min\|\hat{f} - r\|_2\}, \hat{f} \in f, r \in R, \quad (11)$$

$$\hat{f}^*, r^* = \arg \max \arg \min \|\hat{f} - r\|_2, \quad (12)$$

where $R \in \{R_{pc}, R_{rgb}, R_{fs}\}, f \in \{f_{pc}, f_{rgb}, f_{fs}\}$ and η are re-weight parameters.

OCSVM is employed in our model for the ultimate decision-making regarding the segmentation map Seg_m , a renowned anomaly detection algorithm. As noted in PaDim (Defard et al. 2021a), the Mahalanobis distance matrix (MDM) is adept at deriving anomaly scores, hence it is integrated into our model for predicting Sco_a . These two results can be described separately as

$$Sco_a = MDM(S\hat{c}o_a), \quad (13)$$

$$Seg_m = OCSVM(S\hat{e}g_m). \quad (14)$$

Experiments

Experimental Setup

Dataset Construction. The MVTec-3D AD dataset (Bergmann et al. 2022b) is the inaugural multimodal industrial anomaly detection dataset released by MVTec. It encompasses 2656 training samples and 1137 test samples, spanning across 10 industrial entity categories. Alongside the 2D RGB image data of objects within the dataset, high-resolution industrial 3D sensors are employed for depth scanning of products, capturing position information in 3-channel tensors that denote x, y, and z coordinates.

To cater to our research on modality-incomplete in IAD, we restructured the MVTec-3D AD dataset into a modality-incomplete setting, denoted as MIIAD Dataset. In this dataset, modality incompleteness can manifest not only during training but also during testing, with varying degrees of absence for each modality. Employing a random sampler, we constructed our MIIAD Dataset to encompass three types of modality incompleteness: 3D point cloud modality-incomplete, 2D RGB image modality-incomplete, or both modalities-incomplete. For the first two scenarios, for instance, setting the missing rate of 3D point cloud data to $\eta\%$ implies the data comprises solely 2D RGB images of $\eta\%$ and complete data of $(1 - \eta)\%$. Conversely, when the missing rate of 2D RGB image data is $\eta\%$, the situation is reversed. In cases where both modalities are incomplete with a missing rate of $\eta\%$, it signifies the data includes $\frac{\eta}{2}\%$ 2D RGB image data, $\frac{\eta}{2}\%$ 3D point cloud data, and $(1 - \eta)\%$ complete data composition. We followed the settings for modality-missing in recognized works (Wang et al. 2023a; Bao et al. 2022) to ensure the generality of our method.

Evaluation Metrics. All evaluation metrics employed in our experiment align with those provided in the MVTec-3D AD dataset (Bergmann et al. 2022b). To assess anomaly scores, we utilize the pixel-level (P-AUROC) and image-

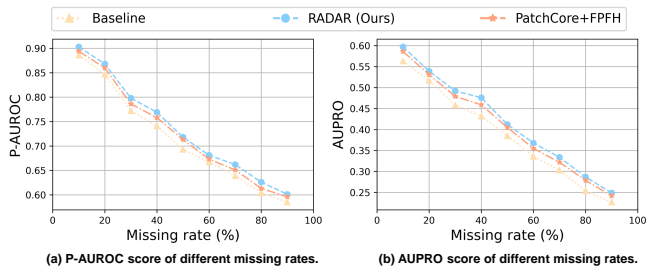


Figure 3: The performance of the framework under various modality missing rates.

level (I-AUROC) area under the receiver operating curve to evaluate pixel-level and image-level anomaly detection performance. In evaluating the segmentation map, we employ the overlap per region (AUPRO) metric.

Implementation Details. Our model’s backbones consist of the following components: i) For 3D point cloud features, extraction is performed by MaskTransformer (Yu et al. 2022) and Point-MAE Decoder (Pang et al. 2022). ii) For 2D RGB image features, ViT (Dosovitskiy et al. 2021) is employed. Specifically, the pre-trained ViTB/8 model with DINO on ImageNet (Deng et al. 2009) serves as our backbone network. Additionally, we have frozen all parameters of the Multimodal Transformer backbone and solely focused on training the parameters associated with MIIAD.

Several learnable modules within RADAR include: i) Modality-incomplete Instruction, with a default length L_i set to 16. The MSA layer index with the prepended instruction ranges from 0 to 3. The optimizer utilized is AdamW, with the learning rate set to 1×10^{-2} . ii) MLP in Instruction Feature Fusion comprises MLP_{rgb} and MLP_{pc} , with AdamW as the optimizer, a learning rate of 1×10^{-3} , and a batch size of 16. iii) The OCSVM in Real-Pseudo Hybrid detection is optimized using SGD, with a learning rate of 1×10^{-4} . Further details are available in the appendix.

Overall Performance

Our framework, RADAR, employs M3DM (Wang et al. 2023b) as the baseline. We conduct comparisons with recent state-of-the-art models on our self-constructed MIIAD Dataset. Tab. 1 presents the experimental outcomes of the P-AUROC metric, while the tables of I-AUROC and AUPRO score results are available in the appendix.

The experimental results demonstrate the effectiveness and robustness of our proposed framework in MIIAD. Firstly, in comparison to the baseline M3DM, our method has notably enhanced performance. For 3D point cloud modality missing rates of 30%, 50%, and 70%, the average P-AUROC metric exhibited improvements of 5.3%, 6.0%, and 7.0%, respectively. Secondly, when compared with other models, our method outperformed in all metrics. In contrast to PatchCore+FPFH model (Horwitz and Hoshen 2022), the P-AUROC values were 5.4%, 5.6%, and 7.5% higher. The significant improvement of I-AUROC and AUPRO metrics is presented in the appendix.

Fig. 3 shows a noticeable decline in the performance of multimodal models as the modality missing rate increases.

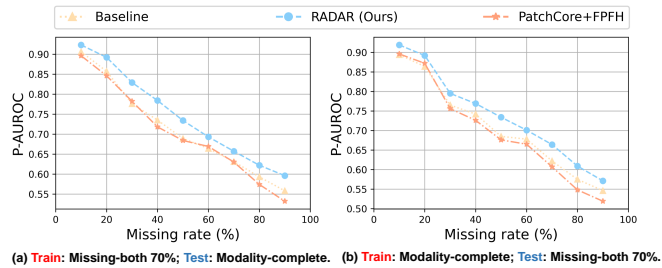


Figure 4: The performance of the framework under various modality missing scenarios.

Table 3: P-AUROC score in comparison with RGB-only, 3D-only, and RGB+3D methods.

Methods		Mean (30% of pc)	Mean (50% of pc)	Mean (70% of pc)
RGB	PADiM (Defard et al. 2021b)	0.654	0.577	0.485
	PatchCore (Roth et al. 2022a)	0.667	0.584	0.493
	STFPM (Wang et al. 2021b)	0.705	0.613	0.548
3D	Depth GAN (Bergmann et al. 2022b)	0.485	0.424	0.379
	Depth VM (Bergmann et al. 2022b)	0.512	0.452	0.403
	3D-ST (Bergmann and Sattlegger 2023b)	0.697	0.614	0.558
	FPFH (Horwitz and Hoshen 2022)	0.724	0.637	0.575
RGB+3D	AST (Rudolph et al. 2023)	0.758	0.668	0.613
	PatchCore+FPFH (Horwitz and Hoshen 2022)	0.771	0.696	0.636
	M3DM (Wang et al. 2023b)	0.772	0.693	0.639
	RADAR (Ours)	0.813	0.735	0.684

However, our method consistently improves the baseline’s performance even as the missing rate rises.

Ablation Study

To evaluate the effectiveness of each module in RADAR, we conducted comprehensive ablation experiments focusing on three key modules: 2D&3D feature extraction (FE), Adaptive Instruction Fusion (AIF), and Real-Pseudo Hybrid Detection (RPHD). Comparing the data in Tab. 2, it is evident that each module we designed enhanced the performance of baseline. The three modules contributed to improvements in the P-AUROC metric by 1.4%, 3.5%, and 2.9%, and in the AUPRO metric by 4.2%, 8.5%, and 10.5%, respectively.

In-Depth Analysis

More comparisons with more RGB-only, 3D-only, and RGB+3D methods. We conducted comparative experiments with RGB-only IAD models, which use only 2D information, and 3D-only IAD models, which rely solely on depth information. From the Tab. 3, it can be seen that the performance of RGB-only and 3D-only models has shown a significant decline on our MIIAD dataset, with our method performing the best among them.

Robustness to missing-modality in different situations.

To evaluate the robustness of our method in various modality-incomplete scenarios during training and testing, we conducted additional experiments.

The experimental outcomes, detailed in Tab. 4, showcase the superiority of our model when the missing rate of 2D RGB image modality or both modalities was set to

Table 4: P-AUROC score for anomaly detection of MIIAD Dataset with RGB image modality or both modalities missing.

Missing type	Methods	MIIAD Dataset										
		Bagel	Cable Gland	Carrot	Cookie	Dowel	Foam	Peach	Potato	Rope	Tire	Mean
RGB Image: 30% 3D Point Cloud: 100%	Voxel GAN (Bergmann et al. 2022b)	0.476	0.453	0.509	0.421	0.406	0.403	0.417	0.454	0.569	0.477	0.446
	Voxel VM (Bergmann et al. 2022b)	0.388	0.376	0.425	0.315	0.327	0.313	0.330	0.329	0.426	0.402	0.341
	PatchCore+FPFH (Horwitz and Hoshen 2022)	0.745	0.701	0.767	0.702	0.699	0.705	0.701	0.732	0.841	0.716	0.725
	AST (Rudolph et al. 2023)	0.748	0.689	0.757	0.706	0.694	0.696	0.683	0.714	0.825	0.697	0.713
	M3DM (Wang et al. 2023b)	0.743	0.705	0.766	0.709	0.708	0.697	0.702	0.747	0.843	0.721	0.728
	RADAR (Ours)	0.780	0.741	0.858	0.749	0.728	0.745	0.746	0.781	0.901	0.752	0.775
RGB Image: 65% 3D Point Cloud: 65%	Voxel GAN (Bergmann et al. 2022b)	0.411	0.388	0.365	0.424	0.403	0.467	0.422	0.387	0.491	0.415	0.395
	Voxel VM (Bergmann et al. 2022b)	0.366	0.342	0.345	0.377	0.369	0.426	0.380	0.361	0.463	0.392	0.351
	PatchCore+FPFH (Horwitz and Hoshen 2022)	0.676	0.639	0.589	0.708	0.579	0.744	0.604	0.577	0.775	0.706	0.658
	AST (Rudolph et al. 2023)	0.652	0.621	0.567	0.675	0.542	0.726	0.587	0.560	0.755	0.679	0.632
	M3DM (Wang et al. 2023b)	0.682	0.638	0.601	0.709	0.579	0.755	0.601	0.576	0.784	0.704	0.663
	RADAR (Ours)	0.725	0.672	0.640	0.764	0.613	0.801	0.624	0.610	0.822	0.744	0.715

Table 5: More P-AUROC score results in different modality-incomplete situations.

Metrics	M3DM (Baseline)	RADAR (Ours)
Mean(modality-complete)	0.926	0.934
Mean(30% of RGB)	0.799	0.852
Mean(50% of RGB)	0.767	0.819
Mean(70% of RGB)	0.728	0.775
Mean(30% of both)	0.746	0.811
Mean(50% of both)	0.705	0.754
Mean(70% of both)	0.663	0.715

70%. Subsequently, we investigated the effects of modality-incomplete at various phases, including scenarios where modality incompleteness occurs during training and completeness during testing, and vice versa, as illustrated by the experimental outcomes in Fig. 4. We further conducted experiments with additional cases of modality missing, with some of the results presented in Tab. 5. These experimental results fully reflect the impressive performance of our framework in various modality-incomplete scenarios, significantly outperforming other methods.

Effect of the position of instruction layers. To deeply analyze the effectiveness of instruction insertion, we visualize the effect of instruction insertion for different transformer layers in Fig. 5. The results indicate the effect of the change of instruction layer on the model performance. It can be observed that inserting modality-incomplete instruction at earlier layers and inserting fewer layers yields better results.

Comparison with modality-incomplete learning methods. To further study the superiority of proposed RADAR, We conducted comparative experiments (Tab. 6 in appendix) with other approaches aiming at addressing modality-missing issues, such as RMT (Ma et al. 2022b), VLMO (Bao et al. 2022), and ShaSpec (Wang et al. 2023a). Not surprisingly, we found that RADAR consistently outperforms existing modality-incomplete learning models by a large margin across all categories. Our intuition is that the one-stage-based methods hardly address the Modality-incomplete issue in industrial anomaly detection scenarios.

Visualization results of IAD. Fig. 6 illustrates our model’s capability in extracting multimodal features. The visualiza-

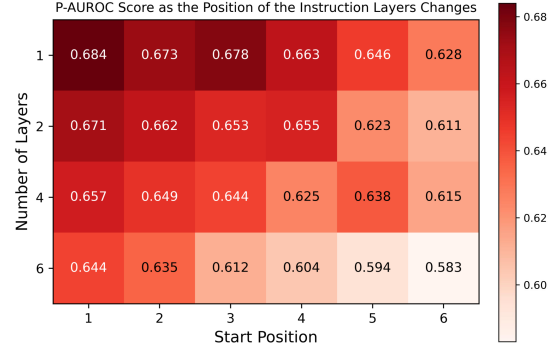


Figure 5: Effect of the position of instruction layers.

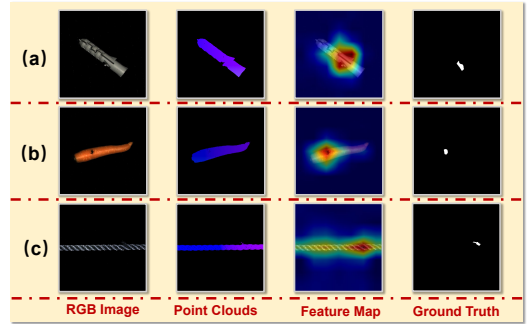


Figure 6: Visualization results of IAD.

tion clearly showcases our model’s aptitude for accurately identifying anomalies across diverse categories.

Conclusion

We propose the first-of-its-kind work to comprehensively investigate the Modality-Incomplete Industrial Anomaly Detection (MIIAD) and construct a novel Robust modALity-aware fusing and Detecting frAMewoRk, abbreviated as **RADAR**. Extensive experiments indicated that our model outperforms other methods on the self-built MIIAD dataset. We believe that the proposed MIIAD task and RADAR serve as a complement to existing literature and provide new insights to the industrial anomaly detection community.

References

- Bao, H.; Wang, W.; Dong, L.; Liu, Q.; Mohammed, O. K.; Aggarwal, K.; Som, S.; Piao, S.; and Wei, F. 2022. VLMO: Unified Vision-Language Pre-Training with Mixture-of-Modality-Experts. In *Advances in Neural Information Processing Systems*.
- Bergmann, P.; Batzner, K.; Fauser, M.; Sattlegger, D.; and Steger, C. 2022a. Beyond dents and scratches: Logical constraints in unsupervised anomaly detection and localization. *International Journal of Computer Vision*, 130(4): 947–969.
- Bergmann, P.; Fauser, M.; Sattlegger, D.; and Steger, C. 2020. Uninformed students: Student-teacher anomaly detection with discriminative latent embeddings. In *Proceedings of the IEEE/CVF conference on computer vision and pattern recognition*, 4183–4192.
- Bergmann, P.; Jin, X.; Sattlegger, D.; and Steger, C. 2022b. The MVTEC 3D-AD Dataset for Unsupervised 3D Anomaly Detection and Localization. In *Proceedings of the 17th International Joint Conference on Computer Vision*, 202–213.
- Bergmann, P.; Löwe, S.; Fauser, M.; Sattlegger, D.; and Steger, C. 2018. Improving unsupervised defect segmentation by applying structural similarity to autoencoders. *arXiv preprint arXiv:1807.02011*.
- Bergmann, P.; and Sattlegger, D. 2023a. Anomaly detection in 3d point clouds using deep geometric descriptors. In *Proceedings of the IEEE/CVF Winter Conference on Applications of Computer Vision*, 2613–2623.
- Bergmann, P.; and Sattlegger, D. 2023b. Anomaly Detection in 3D Point Clouds Using Deep Geometric Descriptors. In *Proceedings of the IEEE/CVF Winter Conference on Applications of Computer Vision (WACV)*, 2613–2623.
- Bonfiglioli, L.; Toschi, M.; Silvestri, D.; Fioraio, N.; and De Gregorio, D. 2022. The Eyecandies Dataset for Unsupervised Multimodal Anomaly Detection and Localization. In *Proceedings of the Asian Conference on Computer Vision (ACCV)*, 3586–3602.
- Chartsias, A.; Joyce, T.; Giuffrida, M. V.; and Tsafaris, S. A. 2017. Multimodal MR synthesis via modality-invariant latent representation. *IEEE transactions on medical imaging*, 37(3): 803–814.
- Chen, C.; Dou, Q.; Jin, Y.; Chen, H.; Qin, J.; and Heng, P.-A. 2019. Robust multimodal brain tumor segmentation via feature disentanglement and gated fusion. In *Medical Image Computing and Computer Assisted Intervention—MICCAI 2019: 22nd International Conference, Shenzhen, China, October 13–17, 2019, Proceedings, Part III* 22, 447–456. Springer.
- Defard, T.; Setkov, A.; Loesch, A.; and Audigier, R. 2021a. PaDiM: A Patch Distribution Modeling Framework for Anomaly Detection and Localization. In *ICPR 2021: Pattern Recognition. ICPR International Workshops and Challenges*, volume 12664, 475–489.
- Defard, T.; Setkov, A.; Loesch, A.; and Audigier, R. 2021b. PaDiM: A Patch Distribution Modeling Framework for Anomaly Detection and Localization. In Del Bimbo, A.; Cucchiara, R.; Sclaroff, S.; Farinella, G. M.; Mei, T.; Bertini, M.; Escalante, H. J.; and Vezzani, R., eds., *Pattern Recognition. ICPR International Workshops and Challenges*, 475–489. Cham: Springer International Publishing. ISBN 978-3-030-68799-1.
- Dehaene, D.; and Eline, P. 2020. Anomaly localization by modeling perceptual features. *arXiv preprint arXiv:2008.05369*.
- Deng, J.; Dong, W.; Socher, R.; Li, L.-J.; Li, K.; and Fei-Fei, L. 2009. Imagenet: A large-scale hierarchical image database. In *IEEE Conference on Computer Vision and Pattern Recognition (CVPR)*, 248–255.
- Dosovitskiy, A.; Beyer, L.; Kolesnikov, A.; Weissenborn, D.; Zhai, X.; Unterthiner, T.; Dehghani, M.; Minderer, M.; Heigold, G.; Gelly, S.; Uszkoreit, J.; and Houlsby, N. 2021. An Image is Worth 16x16 Words: Transformers for Image Recognition at Scale. In *Proceedings of the 9th International Conference on Learning Representations, ICLR 2021*, 3–7.
- Fischler, M. A.; and Bolles, R. C. 1981. Random sample consensus: a paradigm for model fitting with applications to image analysis and automated cartography. *Communications of the ACM*, 24(6): 381–395.
- Gong, X.; Mohan, S.; Dhingra, N.; Bazin, J.-C.; Li, Y.; Wang, Z.; and Ranjan, R. 2023. MMG-Ego4D: Multi-Modal Generalization in Egocentric Action Recognition. In *2023 IEEE/CVF Conference on Computer Vision and Pattern Recognition (CVPR)*, 6481–6491.
- Gudovskiy, D.; Ishizaka, S.; and Kozuka, K. 2022. CFLOW-AD: Real-Time Unsupervised Anomaly Detection with Localization via Conditional Normalizing Flows. In *2022 IEEE/CVF Winter Conference on Applications of Computer Vision (WACV)*, 1819–1828.
- Ha, D.; Dai, A. M.; and Le, Q. V. 2017. HyperNetworks. In *5th International Conference on Learning Representations, ICLR 2017*.
- Horwitz, E.; and Hoshen, Y. 2022. An Empirical Investigation of 3D Anomaly Detection and Segmentation. *arXiv preprint arXiv:2203.05550*.
- Horwitz, E.; and Hoshen, Y. 2023. Back to the feature: classical 3d features are (almost) all you need for 3d anomaly detection. In *Proceedings of the IEEE/CVF Conference on Computer Vision and Pattern Recognition*, 2967–2976.
- Hu, C.; Chen, K.; and Shao, H. 2021. A semantic-enhanced method based on deep SVDD for pixel-wise anomaly detection. In *2021 IEEE International Conference on Multimedia and Expo (ICME)*, 1–6. IEEE.
- Jiang, J.; Zhu, J.; Bilal, M.; Cui, Y.; Kumar, N.; Dou, R.; Su, F.; and Xu, X. 2022. Masked swin transformer unet for industrial anomaly detection. *IEEE Transactions on Industrial Informatics*, 19(2): 2200–2209.
- Karimi Mahabadi, R.; Ruder, S.; Dehghani, M.; and HENDERSON, J. 2021. Parameter-efficient Multi-task Fine-tuning for Transformers via Shared Hypernetworks. In Zong, C.; Xia, F.; Li, W.; and Navigli, R., eds., *Proceedings of the 59th Annual Meeting of the Association for Computational Linguistics and the 11th International Joint Conference on Natural Language Processing (Volume 1: Long Papers)*, 565–576. Online: Association for Computational Linguistics.

- Lee, Y.-L.; Tsai, Y.-H.; Chiu, W.-C.; and Lee, C.-Y. 2023. Multimodal Prompting with Missing Modalities for Visual Recognition. In *IEEE Conference on Computer Vision and Pattern Recognition (CVPR)*.
- Liang, Y.; Zhang, J.; Zhao, S.; Wu, R.; Liu, Y.; and Pan, S. 2023. Omni-frequency channel-selection representations for unsupervised anomaly detection. *IEEE Transactions on Image Processing*.
- Ma, M.; Ren, J.; Zhao, L.; Testuggine, D.; and Peng, X. 2022a. Are multimodal transformers robust to missing modality? In *Proceedings of the IEEE/CVF Conference on Computer Vision and Pattern Recognition*, 18177–18186.
- Ma, M.; Ren, J.; Zhao, L.; Testuggine, D.; and Peng, X. 2022b. Multimodal Prompting with Missing Modalities for Visual Recognition. In *IEEE Conference on Computer Vision and Pattern Recognition (CVPR)*.
- Ma, M.; Ren, J.; Zhao, L.; Tulyakov, S.; Wu, C.; and Peng, X. 2021a. Smil: Multimodal learning with severely missing modality. In *Proceedings of the AAAI Conference on Artificial Intelligence*, volume 35, 2302–2310.
- Ma, M.; Ren, J.; Zhao, L.; Tulyakov, S.; Wu, C.; and Peng, X. 2021b. SMIL: Multimodal Learning with Severely Missing Modality. In *AAAI Conference on Artificial Intelligence (AAAI)*.
- Mishra, P.; Verk, R.; Fornasier, D.; Piciarelli, C.; and Foresti, G. L. 2021. VT-ADL: A vision transformer network for image anomaly detection and localization. In *2021 IEEE 30th International Symposium on Industrial Electronics (ISIE)*, 01–06. IEEE.
- Pang, Y.; Wang, W.; Tay, F. E.; Liu, W.; Tian, Y.; and Yuan, L. 2022. Masked autoencoders for point cloud self-supervised learning. In *Computer Vision—ECCV 2022: 17th European Conference, Tel Aviv, Israel, October 23–27, 2022, Proceedings, Part II*, 604–621. Springer.
- Poklukar, P.; Vasco, M.; Yin, H.; Melo, F. S.; Paiva, A.; and Kragic, D. 2022. Geometric Multimodal Contrastive Representation Learning. *arXiv preprint arXiv:2202.03390*.
- Qi, C. R.; Yi, L.; Su, H.; and Guibas, L. J. 2017. PointNet++: Deep Hierarchical Feature Learning on Point Sets in a Metric Space. In Guyon, I.; Luxburg, U. V.; Bengio, S.; Wallach, H.; Fergus, R.; Vishwanathan, S.; and Garnett, R., eds., *Advances in Neural Information Processing Systems*, volume 30. Curran Associates, Inc.
- Roth, K.; Pemula, L.; Zepeda, J.; Schölkopf, B.; Brox, T.; and Gehler, P. 2022a. Towards Total Recall in Industrial Anomaly Detection. In *Proceedings of the IEEE/CVF Conference on Computer Vision and Pattern Recognition (CVPR)*, 14318–14328.
- Roth, K.; Pemula, L.; Zepeda, J.; Schölkopf, B.; Brox, T.; and Gehler, P. 2022b. Towards Total Recall in Industrial Anomaly Detection. In *IEEE Conference on Computer Vision and Pattern Recognition (CVPR)*, 14318–14328.
- Rudolph, M.; Wehrbein, T.; Rosenhahn, B.; and Wandt, B. 2023. Asymmetric Student-Teacher Networks for Industrial Anomaly Detection. In *Proceedings of the IEEE/CVF Winter Conference on Applications of Computer Vision (WACV)*, 2592–2602.
- Salehi, M.; Sadjadi, N.; Baselizadeh, S.; Rohban, M. H.; and Rabiee, H. R. 2021. Multiresolution knowledge distillation for anomaly detection. In *Proceedings of the IEEE/CVF conference on computer vision and pattern recognition*, 14902–14912.
- Song, J.; Kong, K.; Park, Y.-I.; Kim, S.-G.; and Kang, S.-J. 2021. AnoSeg: Anomaly segmentation network using self-supervised learning. *arXiv preprint arXiv:2110.03396*.
- van den Oord, A.; Li, Y.; and Vinyals, O. 2018. Representation Learning with Contrastive Predictive Coding. *ArXiv*, abs/1807.03748.
- van Tulder, G.; and de Bruijne, M. 2018. Learning cross-modality representations from multi-modal images. *IEEE transactions on medical imaging*, 38(2): 638–648.
- Wang, G.; Han, S.; Ding, E.; and Huang, D. 2021a. Student-teacher feature pyramid matching for anomaly detection. *arXiv preprint arXiv:2103.04257*.
- Wang, G.; Han, S.; Ding, E.; and Huang, D. 2021b. Student-Teacher Feature Pyramid Matching for Anomaly Detection. In *British Machine Vision Conference*.
- Wang, H.; Chen, Y.; Ma, C.; Avery, J.; Hull, L.; and Carneiro, G. 2023a. Multi-modal learning with missing modality via shared-specific feature modelling. In *Proceedings of the IEEE/CVF Conference on Computer Vision and Pattern Recognition*, 15878–15887.
- Wang, L.; Zhang, D.; Guo, J.; and Han, Y. 2020. Image anomaly detection using normal data only by latent space resampling. *Applied Sciences*, 10(23): 8660.
- Wang, Y.; Peng, J.; Zhang, J.; Yi, R.; Wang, Y.; and Wang, C. 2023b. Multimodal industrial anomaly detection via hybrid fusion. In *Proceedings of the IEEE/CVF Conference on Computer Vision and Pattern Recognition*, 8032–8041.
- Wolf, T.; Debut, L.; Sanh, V.; Chaumond, J.; Delangue, C.; Moi, A.; Cistac, P.; Rault, T.; Louf, R.; Funtowicz, M.; Davison, J.; Shleifer, S.; von Platen, P.; Ma, C.; Jernite, Y.; Plu, J.; Xu, C.; Scao, T. L.; Gugger, S.; Drame, M.; Lhoest, Q.; and Rush, A. M. 2020. Transformers: State-of-the-Art Natural Language Processing. In *Proceedings of the 2020 Conference on Empirical Methods in Natural Language Processing: System Demonstrations*, 38–45. Online: Association for Computational Linguistics.
- Wyatt, J.; Leach, A.; Schmon, S. M.; and Willcocks, C. G. 2022. Anoddp: Anomaly detection with denoising diffusion probabilistic models using simplex noise. In *Proceedings of the IEEE/CVF Conference on Computer Vision and Pattern Recognition*, 650–656.
- Yu, X.; Tang, L.; Rao, Y.; Huang, T.; Zhou, J.; and Lu, J. 2022. Point-BERT: Pre-Training 3D Point Cloud Transformers with Masked Point Modeling. In *Proceedings of the IEEE Conference on Computer Vision and Pattern Recognition (CVPR)*.
- Zhang, Y.; Doughty, H.; and Snoek, C. 2023. Learning Unseen Modality Interaction. In Oh, A.; Naumann, T.; Globerson, A.; Saenko, K.; Hardt, M.; and Levine, S., eds., *Advances in Neural Information Processing Systems*, volume 36, 54716–54726. Curran Associates, Inc.

Zhang, Z.; and Deng, X. 2021. Anomaly detection using improved deep SVDD model with data structure preservation. *Pattern Recognition Letters*, 148: 1–6.

Zhao, Z.; Bai, H.; Zhang, J.; Zhang, Y.; Xu, S.; Lin, Z.; Timofte, R.; and Van Gool, L. 2023. CDDFuse: Correlation-Driven Dual-Branch Feature Decomposition for Multi-Modality Image Fusion. In *Proceedings of the IEEE/CVF Conference on Computer Vision and Pattern Recognition (CVPR)*, 5906–5916.

This is the Appendix for paper ‘‘RADAR: Robust Two-stage Modality-incomplete Industrial Anomaly Detection’’. Tab. 6 shows the abbreviations and the symbols used in the main paper.

Table 6: Abbreviations and symbols used in the main paper.

Abbreviation / Symbol	Meaning
<i>Abbreviation</i>	
RADAR	Robust modality-incomplete fusing and detecting framework
MIIAD	Modality-Incomplete Industrial Anomaly Detection
MII	Modality-incomplete Instruction
AIF	Adaptive Instruction Fusion
MLP	Multi-layer perceptron
<i>Symbol in Algorithm</i>	
\mathcal{D}^C	Modality-complete subset data
$\tilde{\mathcal{D}}^{2D}$	3D point cloud modality-incomplete subset data
$\tilde{\mathcal{D}}^{3D}$	2D RGB image modality-incomplete subset data
I_{pc}	MII for 3D point cloud modality-missing
I_{rgb}	MII for 2D RGB image modality-missing
f_{pc}	Features of 3D point clouds
f_{rgb}	Features of 2D RGB images
\oplus	Concatenation
$F_{instruct}$	Modality-incomplete instruction function
HAL	HyperNetwork-based Adaptive Learning
$OCSVM$	One-Class Support Vector Machine
$Maha_{mat}$	Mahalanobis distance matrix

This appendix is organized as follows:

- Section 1 introduces the details of the novel benchmark MIIAD Dataset that we have created.
- Section 2 demonstrates the enhanced efficiency of our RADAR’s parameters following the integration of MII and HyperNetwork.
- Section 3 provides detailed information on the RADAR model construction and training processes not covered in the main paper.
- Section 4 details the AUPRO scores and I-AUROC scores for our RADAR compared to other methods on the MIIAD Dataset, under various 3D point cloud modality missing scenarios.
- Section 5 compares the effectiveness of our modality-incomplete instruction against alternative strategies in addressing modality-missing issue.
- Section 6 presents more detailed results comparing our RADAR with other RGB only, 3D only, and RGB+3D methods.

- Section 7 displays the experimental results of our framework on the Eyecandies dataset (Bonfiglioli et al. 2022).
- Section 8 showcases our model’s visual industrial anomaly detection performance across different categorical objects within the MIIAD Dataset.

Details of MIIAD Dataset

We have developed a novel benchmark called MIIAD Dataset for modality-incomplete industrial anomaly detection task, reconstructed from MVTEC-3D AD dataset (Bergmann et al. 2022b). The dataset contains a total of 10 categories of industrial entities, each consisting of 2D RGB images and 3D point clouds collected using high-resolution industrial 3D sensors.

For each category, there are samples in good condition, as well as abnormal samples aligned with actual industrial testing conditions, such as abrasion, pollution, holes, scratches, etc. In fact, in order to meet the needs of different modality incomplete scenarios, we have established sub-datasets with different degrees of modality missing. Tab. 7 displays more statistical information for datasets with missing rates of 70% for 3D point cloud modality.

Efficiency on Parameters

We have integrated HyperNetwork (Ha, Dai, and Le 2017) to dynamically cater to tasks with fewer parameters, aiming for enhanced performance (Karimi Mahabadi et al. 2021). During the training of our modality-incomplete instruction, we leveraged prompt learning by freezing all parameters of the simple Multimodal Transformer, retaining only the MLP and fully connected layer for downstream task processing. Consequently, the number of parameters that our model RADAR requires to train is significantly reduced. As illustrated in the Tab. 8, in contrast to the 510M parameter count in the Unsupervised Feature Fusion (UFF) module of the Baseline model M3DM (Wang et al. 2023b), our model only necessitates training 6,842K parameter counts, representing merely 1.34%. Nonetheless, our model’s performance significantly exceeds that of the Baseline.

Table 7: Details of MIIAD Dataset with 70% missing rate for 3D point cloud modality.

Category	RGB iamges in # Train	Point clouds in # Train	RGB iamges in # Test	Point clouds in # Test	Anomaly types	Image size (width × height)
bagel	244	74	110	33	4	800 × 800
cable gland	223	67	108	33	4	400 × 400
carrot	286	86	159	48	5	800 × 800
cookie	210	63	131	40	4	500 × 500
dowel	288	87	130	39	4	400 × 400
foam	236	71	100	30	4	900 × 900
peach	361	109	132	40	5	600 × 600
potato	300	90	114	35	4	800 × 800
rope	298	90	101	31	3	900 × 400
tire	210	63	112	34	4	600 × 800
total	2656	800	1197	363	41	

Table 8: Comparison of parameter efficiency.

Methods	# Trained params	Relative proportion	MIIAD Dataset										
			Bagel	Cable Gland	Carrot	Cookie	Dowel	Foam	Peach	Potato	Rope	Tire	Mean
M3DM (Baseline) (Wang et al. 2023b)	510,603K	100%	0.613	0.620	0.689	0.634	0.636	0.647	0.594	0.629	0.702	0.578	0.639
RADAR (Ours)	6,842K	1.34%	0.653	0.624	0.723	0.670	0.661	0.705	0.630	0.645	0.741	0.617	0.684

Algorithm 1: Robust modality-incomplete fusing and detecting framework (RADAR)

Input: Multimodal data samples
 $\tilde{\mathcal{D}} = \{\mathcal{D}^C, \tilde{\mathcal{D}}^{2D}, \tilde{\mathcal{D}}^{3D}\}$ from MIIAD Dataset;
Output: Segmentation map Seg_m and anomaly score Sco_a .

for $d_{pc}, d_{rgb} \in \tilde{\mathcal{D}}$ **do**
 if d_{pc} **is incomplete then**
 $I_{m1} = I_{pc}$;
 else
 f_{pc} is obtained from F_{pc} ;
 if d_{rgb} **is incomplete then**
 $I_{m2} = I_{rgb}$;
 else
 f_{rgb} is obtained from F_{rgb} ;
 $T_{fs} = f_{pc} \oplus f_{rgb}$;
 if I_{m1} **is not None then**
 $T_{ex} = F_{instruct}(I_{m1}, T_{fs})$;
 else if I_{m2} **is not None then**
 $T_{ex} = F_{instruct}(I_{m2}, T_{fs})$;
 else
 $T_{ex} = T_{fs}$;
 $\{\hat{f}_{pc}, \hat{f}_{rgb}\} = T_{ex}$;
 $\{g_{pc}, g_{rgb}, g_{fs}\} = HAL(\{\hat{f}_{pc}, \hat{f}_{rgb}\})$;
 $Seg_m =$
 $OCSVM(\{\psi(R_{pc}, g_{pc}), \psi(R_{rgb}, g_{rgb}), \psi(R_{fs}, g_{fs})\})$;
 $Sco_a =$
 $MDM(\{\phi(R_{pc}, g_{pc}), \phi(R_{rgb}, g_{rgb}), \phi(R_{fs}, g_{fs})\})$;
return Segmentation map and anomaly score.

Implementation Details

The pseudocode of the process of our model RADAR can be represented by Algorithm 1.

During the data reading phase, for instances with incomplete 3D point cloud modality where point cloud information is encapsulated in TIFF format, we generate a tensor filled with ones, matching the size of the read data, to serve as a pseudo input (i.e. \tilde{x}^{m_1}). For cases with incomplete 2D RGB image modality, we employ images where all pixel values are set to one to act as pseudo inputs (i.e. \tilde{x}^{m_2}). We apply RANSAC (Fischler and Bolles 1981) for estimating the background plane in 3D point cloud data, eliminating points within a 0.005 distance threshold, and subsequently

resizing both the position tensor and the 2D RGB image to a 224×224 patch. We employ a hybrid of MaskTransformer (Yu et al. 2022) and Point-MAE Decoder (Pang et al. 2022) to extract features from 3D point clouds. In reference to (Wang et al. 2023b), the outputs from the $\{3, 7, 11\}$ layers are converted into x, y, and z coordinates to represent three-dimensional features, respectively.

AUPRO and I-AUROC scores for MIIAD

In addition to the P-AUROC score mentioned in the main paper, Tab. 9 and Tab. 10 display the experimental results for the AUPRO metric and I-AUROC metric on the MIIAD Dataset under conditions of 3D point cloud modality absence to show more details of our experiments.

Specifically, the AUPRO scores of our framework exceed those of the second-best method, by 13.1%, 13.4%, and 21.4% at 3D point cloud modality missing rates of 30%, 50%, and 70%, correspondingly. And the I-AUROC scores exceed the second-best method by 4.1%, 6.1%, and 5.2%. These results demonstrate our strategy’s robustness and effectiveness, surpassing competing approaches.

Comparison with other methods tackling modality-incomplete issue

In the main paper, we primarily focused on comparing the performance of our method against the current leading industrial anomaly detection models in the MIIAD task. To highlight the advanced nature of our approach to handling modality-incomplete instruction, we conducted comparative experiments with other methods designed to tackle the issue of modality-missing. The methods compared are as follows:

SMIL (Ma et al. 2021b) incorporates Bayesian meta-learning to explore the potential feature space, aiming to align the features of an incomplete mode with those of a complete mode.

GMC (Poklukar et al. 2022) has devised a geometric multimodal contrastive learning approach to tackle the challenge of inherent heterogeneity in multimodal learning.

RMT (Ma et al. 2022b) addresses various modality-missing scenarios through automatic search and incorporates task tokens to optimize cross-modal.

VLMO (Bao et al. 2022) introduces a hybrid multimodal expert model that leverages both the Dual Encoder for image retrieval tasks and the Fusion Encoder for multimodal encoding.

ShaSpec (Wang et al. 2023a) has devised a ”Shared Specific Feature Modeling” method focused on learning shared and specific features across multimodal data to address missing modality representations.

Table 9: AUPRO score for anomaly detection of MIIAD Dataset with 3D point cloud modality missing. A larger score indicates better performance. We color each row as the **best, **second best**, and **third best**.**

Missing rate	Methods	MIIAD Dataset										
		Bagel	Cable Gland	Carrot	Cookie	Dowel	Foam	Peach	Potato	Rope	Tire	Mean
30%	Voxel GAN (Bergmann et al. 2022b)	0.324	0.386	0.434	0.392	0.335	0.314	0.307	0.391	0.384	0.368	0.357
	Voxel VM (Bergmann et al. 2022b)	0.289	0.343	0.377	0.346	0.302	0.278	0.283	0.336	0.342	0.315	0.316
	PatchCore+FPFH (Horwitz and Hoshen 2022)	0.402	0.490	0.545	0.526	0.443	0.407	0.394	0.467	0.452	0.448	0.454
	AST (Rudolph et al. 2023)	0.398	0.479	0.542	0.515	0.447	0.405	0.386	0.460	0.447	0.443	0.449
	M3DM (Wang et al. 2023b)	0.394	0.491	0.544	0.517	0.450	0.424	0.389	0.456	0.463	0.451	0.458
	RADAR (Ours)	0.462	0.532	0.580	0.552	0.541	0.464	0.456	0.553	0.542	0.475	0.518
50%	Voxel GAN (Bergmann et al. 2022b)	0.276	0.254	0.397	0.379	0.332	0.345	0.267	0.313	0.388	0.265	0.296
	Voxel VM (Bergmann et al. 2022b)	0.243	0.231	0.346	0.328	0.289	0.311	0.224	0.287	0.360	0.221	0.258
	PatchCore+FPFH (Horwitz and Hoshen 2022)	0.365	0.318	0.470	0.449	0.407	0.419	0.323	0.365	0.423	0.314	0.387
	AST (Rudolph et al. 2023)	0.352	0.296	0.453	0.438	0.399	0.410	0.312	0.347	0.406	0.293	0.363
	M3DM (Wang et al. 2023b)	0.366	0.317	0.466	0.458	0.411	0.415	0.322	0.369	0.412	0.317	0.385
	RADAR (Ours)	0.398	0.372	0.528	0.490	0.454	0.457	0.357	0.451	0.482	0.347	0.439
70%	Voxel GAN (Bergmann et al. 2022b)	0.203	0.276	0.344	0.265	0.277	0.303	0.201	0.312	0.268	0.227	0.256
	Voxel VM (Bergmann et al. 2022b)	0.176	0.243	0.301	0.216	0.243	0.276	0.166	0.278	0.230	0.198	0.227
	PatchCore+FPFH (Horwitz and Hoshen 2022)	0.257	0.312	0.374	0.318	0.317	0.336	0.249	0.338	0.297	0.254	0.302
	AST (Rudolph et al. 2023)	0.226	0.297	0.361	0.298	0.301	0.315	0.222	0.316	0.259	0.223	0.279
	M3DM (Wang et al. 2023b)	0.253	0.316	0.374	0.307	0.325	0.330	0.247	0.341	0.302	0.259	0.303
	RADAR (Ours)	0.304	0.350	0.428	0.356	0.354	0.365	0.304	0.390	0.342	0.343	0.368

Table 10: I-AUROC score for anomaly detection of MIIAD Dataset with 3D point cloud modality missing.

Missing rate	Methods	MIIAD Dataset										
		Bagel	Cable Gland	Carrot	Cookie	Dowel	Foam	Peach	Potato	Rope	Tire	Mean
30%	Voxel GAN (Bergmann et al. 2022b)	0.716	0.687	0.713	0.667	0.698	0.570	0.646	0.588	0.748	0.574	0.676
	Voxel VM (Bergmann et al. 2022b)	0.593	0.578	0.602	0.586	0.643	0.484	0.573	0.506	0.655	0.467	0.557
	PatchCore+FPFH (Horwitz and Hoshen 2022)	0.924	0.854	0.858	0.844	0.863	0.797	0.837	0.726	0.893	0.740	0.834
	AST (Rudolph et al. 2023)	0.916	0.838	0.860	0.815	0.832	0.792	0.816	0.704	0.885	0.719	0.818
	M3DM (Wang et al. 2023b)	0.932	0.857	0.871	0.835	0.848	0.814	0.843	0.725	0.906	0.732	0.842
	RADAR (Ours)	0.954	0.887	0.903	0.859	0.891	0.843	0.878	0.747	0.933	0.763	0.877
50%	Voxel GAN (Bergmann et al. 2022b)	0.667	0.586	0.631	0.596	0.643	0.556	0.625	0.498	0.690	0.503	0.595
	Voxel VM (Bergmann et al. 2022b)	0.587	0.495	0.554	0.521	0.574	0.425	0.518	0.412	0.608	0.442	0.512
	PatchCore+FPFH (Horwitz and Hoshen 2022)	0.893	0.746	0.860	0.722	0.803	0.776	0.808	0.646	0.886	0.683	0.768
	AST (Rudolph et al. 2023)	0.862	0.752	0.831	0.716	0.788	0.759	0.784	0.627	0.859	0.669	0.744
	M3DM (Wang et al. 2023b)	0.887	0.761	0.847	0.747	0.815	0.778	0.807	0.654	0.877	0.694	0.783
	RADAR (Ours)	0.918	0.792	0.882	0.783	0.852	0.812	0.838	0.683	0.905	0.727	0.831
70%	Voxel GAN (Bergmann et al. 2022b)	0.612	0.443	0.657	0.478	0.605	0.560	0.562	0.452	0.646	0.449	0.523
	Voxel VM (Bergmann et al. 2022b)	0.506	0.368	0.576	0.398	0.497	0.495	0.482	0.334	0.527	0.366	0.415
	PatchCore+FPFH (Horwitz and Hoshen 2022)	0.830	0.662	0.798	0.627	0.795	0.732	0.768	0.609	0.855	0.651	0.708
	AST (Rudolph et al. 2023)	0.812	0.638	0.784	0.619	0.776	0.735	0.755	0.572	0.832	0.636	0.592
	M3DM (Wang et al. 2023b)	0.843	0.654	0.804	0.643	0.786	0.748	0.776	0.598	0.849	0.667	0.719
	RADAR (Ours)	0.879	0.677	0.836	0.701	0.824	0.774	0.805	0.663	0.871	0.695	0.757

Tab. 11 displays the experimental results, highlighting that our modality-incomplete instruction significantly outshines recent methods designed to tackle modality-missing issues. Taking our top-performing input-level instruction as an example, it boasts an average P-AUROC metric that is 4.7%, 4.7%, and 6.3% higher than the runner-up, ShaSpec (Wang et al. 2023a), at 3D point cloud modality missing rates of 30%, 50%, and 70%, respectively. This un-

derscores the superiority and robustness of our approach.

Detailed comparisons with more RGB-only, 3D-only, and RGB+3D methods

We conducted comparative experiments with RGB-only IAD models, which use only 2D information, and 3D-only IAD models, which rely solely on depth information. Tab. 12 showcases more detailed results. It can be seen that the

Table 11: P-AUROC score for anomaly detection in MIAD Dataset with 3D point cloud modality missing based on methods aiming at addressing modality-incomplete issue.

Missing rate	Methods	MIAD Dataset										
		Bagel	Cable Gland	Carrot	Cookie	Dowel	Foam	Peach	Potato	Rope	Tire	Mean
30%	SMIL (Ma et al. 2021b)	0.731	0.733	0.758	0.756	0.724	0.735	0.702	0.726	0.810	0.731	0.733
	GMC (Poklukar et al. 2022)	0.742	0.759	0.786	0.772	0.751	0.743	0.724	0.757	0.821	0.758	0.760
	RMT (Ma et al. 2022b)	0.738	0.765	0.784	0.776	0.748	0.752	0.729	0.768	0.829	0.762	0.763
	VLMO (Bao et al. 2022)	0.751	0.783	0.780	0.769	0.752	0.738	0.718	0.766	0.836	0.765	0.769
	ShaSpec (Wang et al. 2023a)	0.756	0.779	0.794	0.776	0.750	0.749	0.736	0.773	0.838	0.774	0.776
	RADAR (Ours)	0.794	0.803	0.832	0.805	0.784	0.769	0.758	0.811	0.872	0.797	0.813
50%	SMIL (Ma et al. 2021b)	0.645	0.613	0.712	0.708	0.626	0.692	0.621	0.654	0.744	0.629	0.653
	GMC (Poklukar et al. 2022)	0.652	0.631	0.729	0.737	0.654	0.703	0.626	0.709	0.763	0.657	0.678
	RMT (Ma et al. 2022b)	0.648	0.635	0.736	0.733	0.667	0.709	0.630	0.718	0.759	0.665	0.686
	VLMO (Bao et al. 2022)	0.662	0.644	0.739	0.741	0.663	0.707	0.637	0.724	0.769	0.683	0.694
	ShaSpec (Wang et al. 2023a)	0.667	0.653	0.742	0.737	0.678	0.706	0.645	0.720	0.766	0.688	0.702
	RADAR (Ours)	0.713	0.673	0.752	0.773	0.752	0.719	0.682	0.750	0.794	0.723	0.735
70%	SMIL (Ma et al. 2021b)	0.553	0.584	0.674	0.633	0.589	0.616	0.577	0.592	0.678	0.537	0.602
	GMC (Poklukar et al. 2022)	0.598	0.604	0.682	0.643	0.621	0.627	0.601	0.606	0.694	0.558	0.628
	RMT (Ma et al. 2022b)	0.597	0.615	0.680	0.641	0.632	0.635	0.598	0.617	0.703	0.565	0.632
	VLMO (Bao et al. 2022)	0.614	0.608	0.696	0.637	0.638	0.656	0.604	0.623	0.716	0.582	0.639
	ShaSpec (Wang et al. 2023a)	0.618	0.613	0.692	0.647	0.642	0.648	0.609	0.625	0.713	0.589	0.643
	RADAR (Ours)	0.653	0.624	0.723	0.670	0.661	0.705	0.630	0.645	0.741	0.617	0.684

Table 12: P-AUROC score in comparison with RGB-only, 3D-only, and RGB+3D methods.

Missing rate	Methods	MIAD Dataset											
		Bagel	Cable Gland	Carrot	Cookie	Dowel	Foam	Peach	Potato	Rope	Tire	Mean	
30%	RGB	PADiM (Defard et al. 2021b)	0.657	0.662	0.684	0.631	0.674	0.627	0.632	0.692	0.725	0.682	0.654
		PatchCore (Roth et al. 2022a)	0.645	0.681	0.685	0.642	0.681	0.645	0.621	0.689	0.722	0.668	0.667
		STFPM (Wang et al. 2021b)	0.678	0.701	0.726	0.687	0.707	0.677	0.653	0.714	0.743	0.695	0.705
	3D	Depth GAN (Bergmann et al. 2022b)	0.492	0.495	0.531	0.515	0.478	0.465	0.498	0.466	0.587	0.467	0.485
		3D-ST (Bergmann and Sattlegger 2023b)	0.687	0.687	0.705	0.694	0.688	0.672	0.650	0.699	0.752	0.687	0.697
		FPFH (Horwitz and Hoshen 2022)	0.703	0.726	0.749	0.712	0.723	0.697	0.677	0.726	0.776	0.714	0.724
	RGB+3D	PatchCore+FPFH (Horwitz and Hoshen 2022)	0.758	0.779	0.797	0.776	0.755	0.752	0.729	0.776	0.832	0.765	0.771
		M3DM (Wang et al. 2023b)	0.754	0.782	0.795	0.783	0.747	0.755	0.731	0.777	0.835	0.763	0.772
		RADAR (Ours)	0.794	0.803	0.832	0.805	0.784	0.769	0.758	0.811	0.872	0.797	0.813
70%	RGB	PADiM (Defard et al. 2021b)	0.485	0.477	0.580	0.510	0.541	0.556	0.478	0.502	0.543	0.397	0.485
		PatchCore (Roth et al. 2022a)	0.477	0.483	0.579	0.521	0.534	0.549	0.501	0.509	0.552	0.416	0.493
		STFPM (Wang et al. 2021b)	0.527	0.538	0.615	0.557	0.551	0.572	0.514	0.553	0.610	0.478	0.548
	3D	Depth GAN (Bergmann et al. 2022b)	0.379	0.384	0.415	0.405	0.398	0.430	0.351	0.380	0.487	0.387	0.379
		3D-ST (Bergmann and Sattlegger 2023b)	0.554	0.558	0.658	0.587	0.553	0.591	0.532	0.558	0.637	0.502	0.558
		FPFH (Horwitz and Hoshen 2022)	0.568	0.565	0.642	0.588	0.574	0.604	0.544	0.574	0.641	0.519	0.575
	RGB+3D	PatchCore+FPFH (Horwitz and Hoshen 2022)	0.610	0.617	0.691	0.627	0.635	0.652	0.593	0.622	0.696	0.585	0.636
		M3DM (Wang et al. 2023b)	0.613	0.620	0.689	0.634	0.636	0.647	0.594	0.629	0.702	0.578	0.639
		RADAR (Ours)	0.653	0.624	0.723	0.670	0.661	0.705	0.630	0.645	0.741	0.617	0.684

performance of RGB-only and 3D-only models has shown a significant decline on our MIAD dataset, with our method performing the best among them.

Modality-incomplete industrial anomaly detection results on Eyecandies dataset

To demonstrate the broad applicability of our method, we also conducted experiments on the Eyecandies dataset (Bon-

Table 13: P-AUROC score for anomaly detection of Eyecandies dataset with 3D point cloud modality missing.

Missing rate	Methods	Eyecandies dataset										Mean
		Candy Cane	Chocolate Cookie	Chocolate Praline	Confetto	Gummy Bear	Hazelnut Truffle	Licorice Sandwich	Lollipop	Marsh-mallow	Papermint Candy	
30%	PatchCore+FPFH (Horwitz and Hoshen 2022)	0.773	0.797	0.676	0.836	0.738	0.589	0.782	0.743	0.843	0.817	0.748
	AST (Rudolph et al. 2023)	0.752	0.794	0.641	0.832	0.707	0.561	0.746	0.730	0.819	0.796	0.724
	M3DM (Wang et al. 2023b)	0.787	0.812	0.687	0.857	0.743	0.578	0.776	0.762	0.857	0.823	0.754
	RADAR (Ours)	0.832	0.841	0.735	0.891	0.774	0.624	0.812	0.810	0.894	0.876	0.805
50%	PatchCore+FPFH (Horwitz and Hoshen 2022)	0.719	0.758	0.654	0.732	0.664	0.503	0.694	0.703	0.809	0.741	0.661
	AST (Rudolph et al. 2023)	0.695	0.716	0.626	0.743	0.645	0.482	0.677	0.681	0.765	0.726	0.636
	M3DM (Wang et al. 2023b)	0.724	0.747	0.651	0.760	0.672	0.501	0.706	0.717	0.805	0.759	0.668
	RADAR (Ours)	0.768	0.779	0.682	0.816	0.703	0.568	0.745	0.749	0.836	0.815	0.732
70%	PatchCore+FPFH (Horwitz and Hoshen 2022)	0.653	0.662	0.587	0.672	0.571	0.456	0.656	0.607	0.701	0.687	0.603
	AST (Rudolph et al. 2023)	0.638	0.612	0.576	0.643	0.554	0.409	0.627	0.573	0.687	0.683	0.578
	M3DM (Wang et al. 2023b)	0.652	0.649	0.592	0.697	0.583	0.449	0.653	0.599	0.726	0.701	0.611
	RADAR (Ours)	0.716	0.725	0.635	0.754	0.638	0.504	0.702	0.668	0.778	0.762	0.676

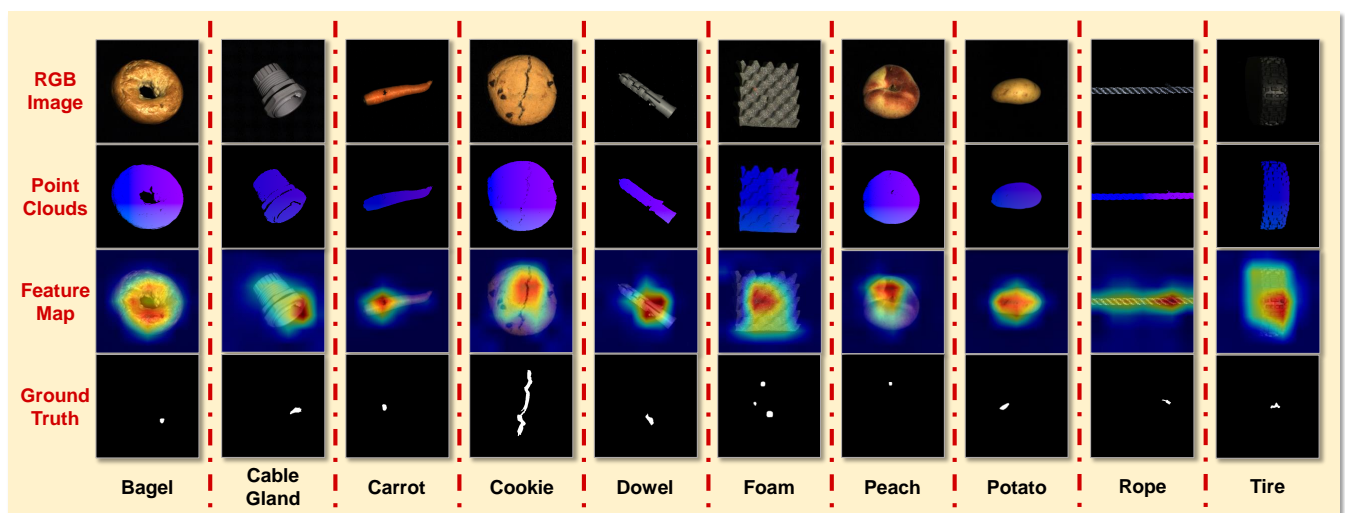


Figure 7: Additional visualization results of industrial anomaly detection.

figlioli et al. 2022). The experimental results are shown in the Tab. 13. As can be seen from the table, our method still performs competitively on the Eyecandies dataset with more complex cases, outperforming other models.

Additional Visualization Results

As depicted in Fig. 7, we present additional industrial anomaly results for all categories within the MIIAD Dataset. As can be seen from the figure, for each category of the dataset, our model can identify abnormal industrial entities while accurately locating the position of anomalies.